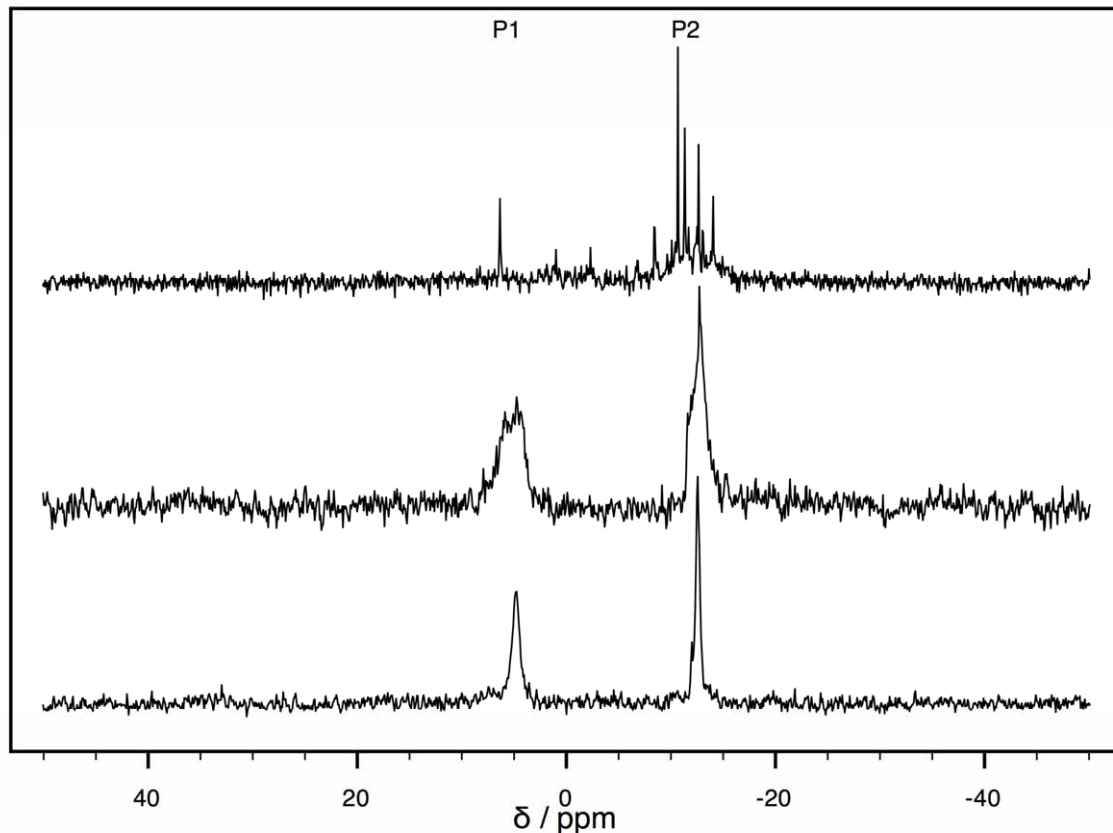


Electronic Supplementary Information for

**Series Behavior of Lanthanoid(III) Complexes with the  $\alpha$ -1-Wells-Dawson Heteropolyoxoanion in Acetonitrile: Electrochemistry and Ln Coordination<sup>†</sup>**

Mark R. Antonio <sup>\*,‡</sup>, Jing Jing, <sup>§</sup> Benjamin P. Burton-Pye, <sup>§</sup> Lynn C. Francesconi <sup>\*,§</sup>

<sup>‡</sup>Chemical Sciences & Engineering Division, Argonne National Laboratory, Argonne, Illinois 60439, <sup>§</sup>Department of Chemistry, Hunter College and the Graduate School of the City University of New York, New York, New York 10021



**Figure S1.**  $^{31}\text{P}$  NMR spectrum of 20 mM  $\text{TBA}^+$ -Eu- $\alpha$ -1 in dry,  $d^3$  acetonitrile (top), and after additions of 2%  $\text{H}_2\text{O}$  (middle), and 10%  $\text{H}_2\text{O}$  (bottom). P1 denotes the phosphate resonance near the lacuna and P2 denotes the remote phosphate resonance.

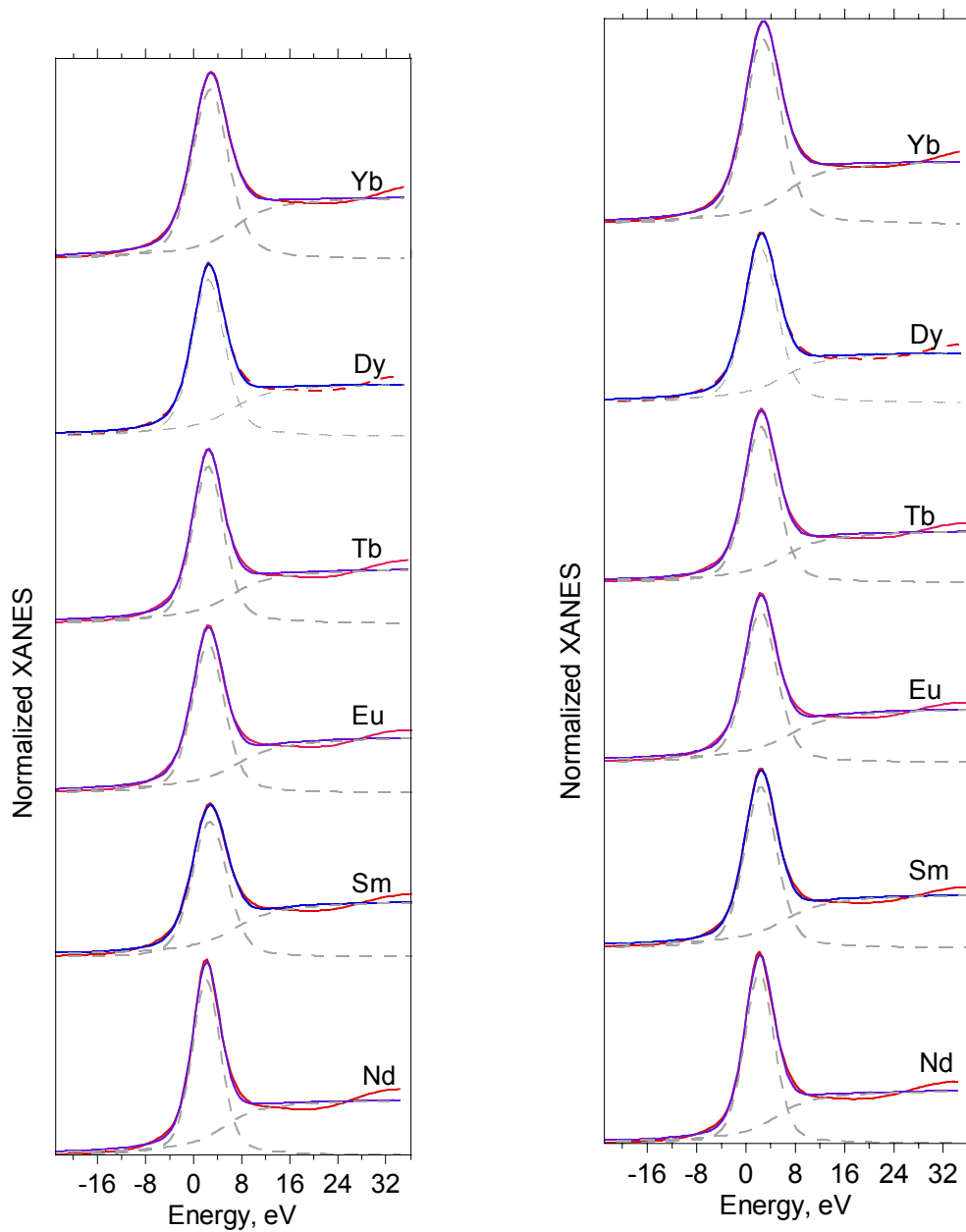


**Figure S2.** The normalized, experimental XANES (red solid line) for the  $\text{TBA}^+ \text{-Ln-}\alpha\text{-1}$  solid salts (left) and their 4.3 mM solutions (right) in the acetonitrile electrolyte (0.1 M  $\text{TBAPF}_6$ ). The fits to the data are shown as blue solid lines. The individual pseudo-Voigt and arctangent function of the fits are shown as grey dashed lines.

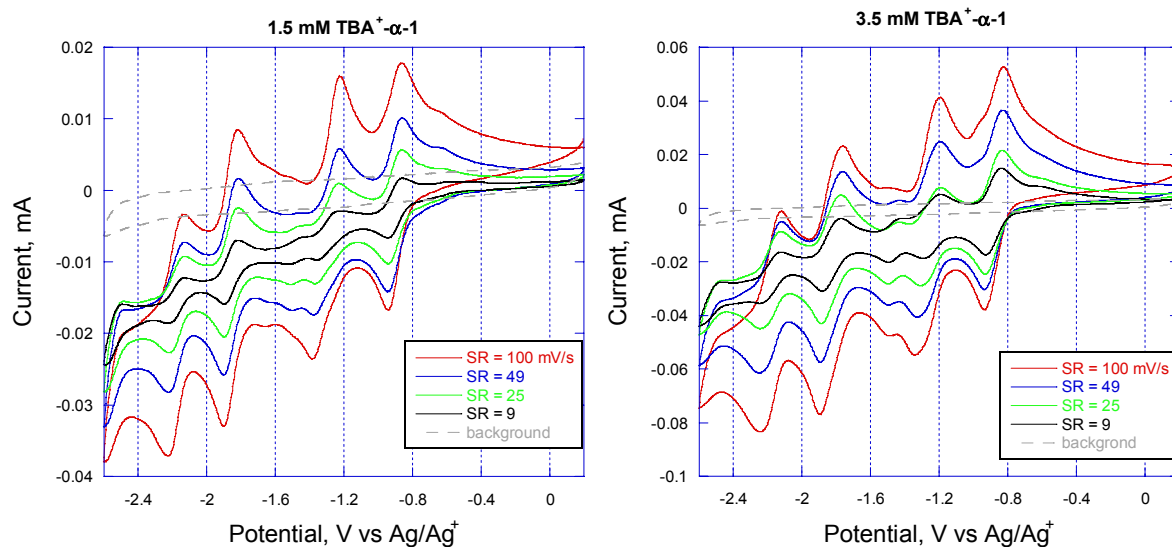


**Figure S3.** Cyclic voltammograms of 1.5 mM (left) and 3.5 mM (right) solution concentrations of the TBA<sup>+</sup> salt of  $\alpha$ -1-[P<sub>2</sub>W<sub>17</sub>O<sub>61</sub>]<sup>10-</sup> in dry CH<sub>3</sub>CN with 0.1 M TBAPF<sub>6</sub> electrolyte obtained with a GC electrode working electrode and different scan rates in mV s<sup>-1</sup>, starting at +0.2 V. The background scan in the absence of analyte is shown as the grey dashed line.

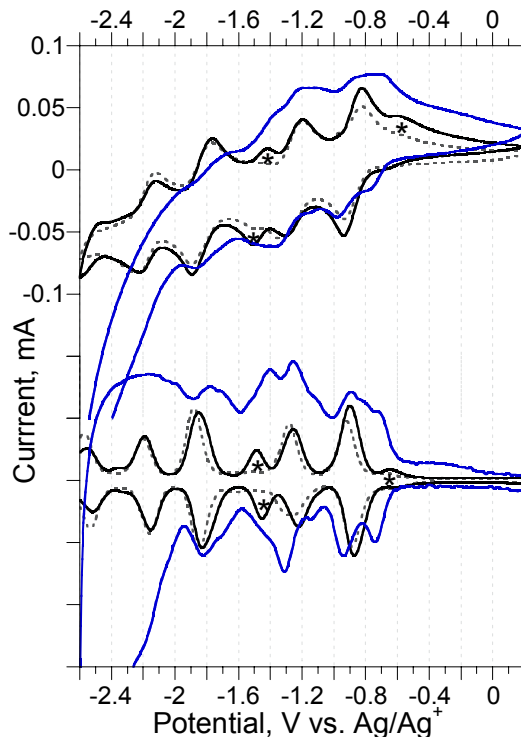


**Figure S4.** CV (top) and DPV (bottom) of the TBA<sup>+</sup> salt for a fresh 3.5 mM solution of  $\alpha$ -1-[P<sub>2</sub>W<sub>17</sub>O<sub>61</sub>]<sup>10-</sup> (dashed lines) in MeCN with 0.1 M TBAPF<sub>6</sub> electrolyte and after

cycling for an hour (solid black lines) at  $v = 20 \text{ mV s}^{-1}$  showing the development of new couples (identified with asterisks) and after the deliberate addition of  $\text{H}_2\text{O}$  (blue lines) for which, in the absence of DPV data, the semi-differential (convolution) data of the CV are shown.

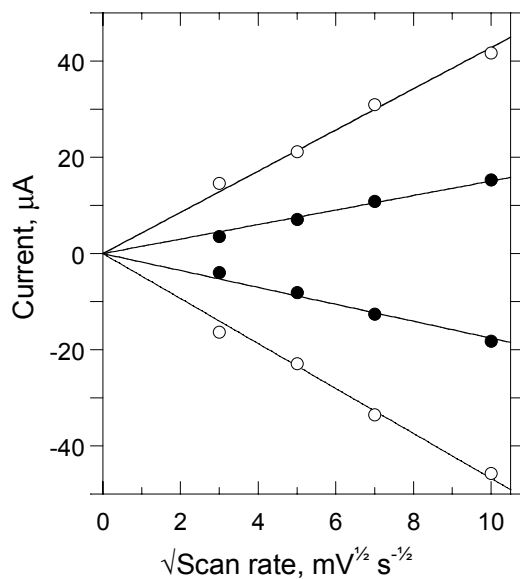


**Figure S5.** Anodic and cathodic peak current,  $i_{\text{pa}}$  and  $i_{\text{pc}}$ , variations of the first redox couple with the square roots of scan rates ( $v = 9, 25, 49, \text{ and } 100 \text{ mV s}^{-1}$ ) from the CVs of Figure S3 for 1.5 mM (solid circles) and 3.5 mM (open circles)  $\alpha 1\text{-[P}_2\text{W}_{17}\text{O}_{61}]^{10-}$  analyte concentrations. The fitted lines with intercepts of zero are based upon the Randles-Sevcik equation,  $i_p = (5.02RT)^{-1/2}(nF)^{3/2}ACD^{1/2}v^{1/2}$  with the conventional symbol meanings.<sup>1</sup> The slopes are -1.76(7) and -4.7(1) for the  $i_{\text{pc}}$  response (1.5 and 3.5 mM, respectively) and 1.51(5) and 4.3(1) for  $i_{\text{pa}}$  (1.5 and 3.5 mM, respectively). The regression coefficients ( $R^2$ ) for the fits are 0.976–0.987. At the 1.5 mM analyte concentration, the average  $i_{\text{pa}}/i_{\text{pc}}$  ratio is -0.86 and at 3.5 mM, the corresponding value is -0.92.

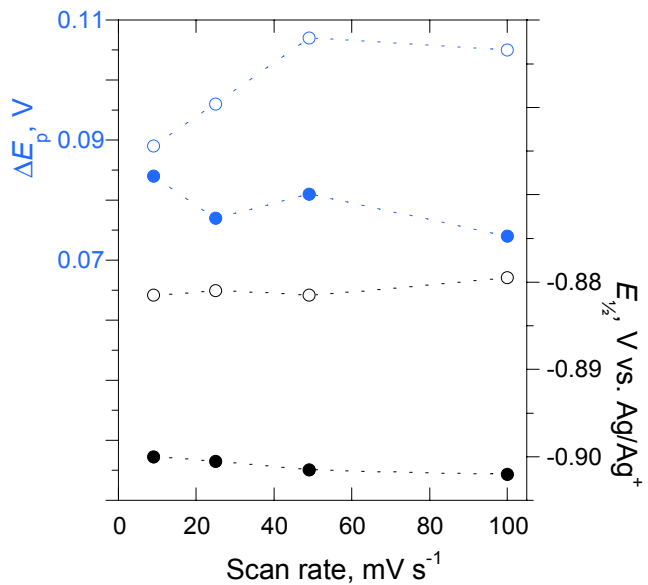


**Figure S6.** Peak separations,  $\Delta E_p = E_{pa} - E_{pc}$  (left, blue ordinate), and half-wave potentials,  $E_{1/2} = (E_{pa} + E_{pc})/2$  (right, black ordinate), for the first redox couple obtained from the CV data of Figure S3 and their variations with scan rates ( $v = 9, 25, 49$ , and  $100$  mV s<sup>-1</sup>) for  $1.5$  mM (solid circles) and  $3.5$  mM (open circles)  $\alpha 1\text{-}[P_2W_{17}O_{61}]^{10-}$  analyte concentrations.

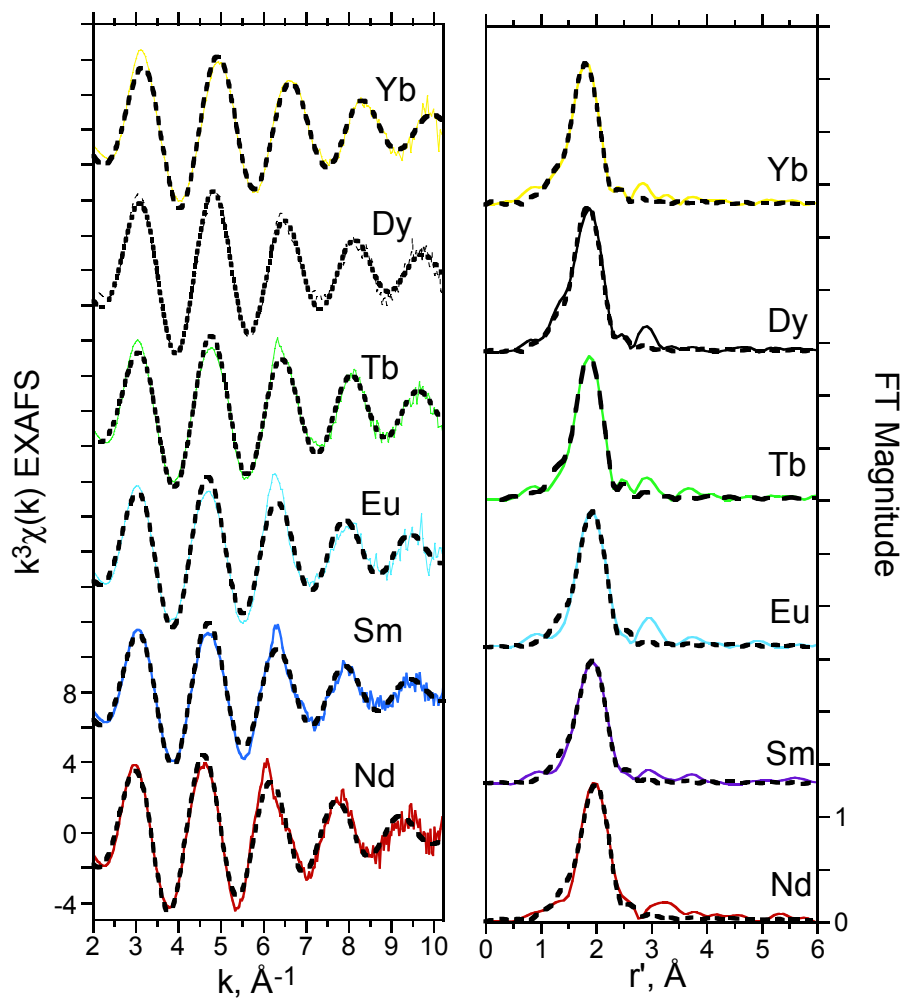


**Figure S7a.** The Ln L<sub>3</sub>-edge  $k^3\chi(k)$  EXAFS data and corresponding FT data for the neat TBA<sup>+</sup>-Ln- $\alpha$ -1 salts. The experimental data are shown as solid lines and the fits obtained by using the one O-shell model are shown as dashed lines. The metrical parameters are provided in Table S1.

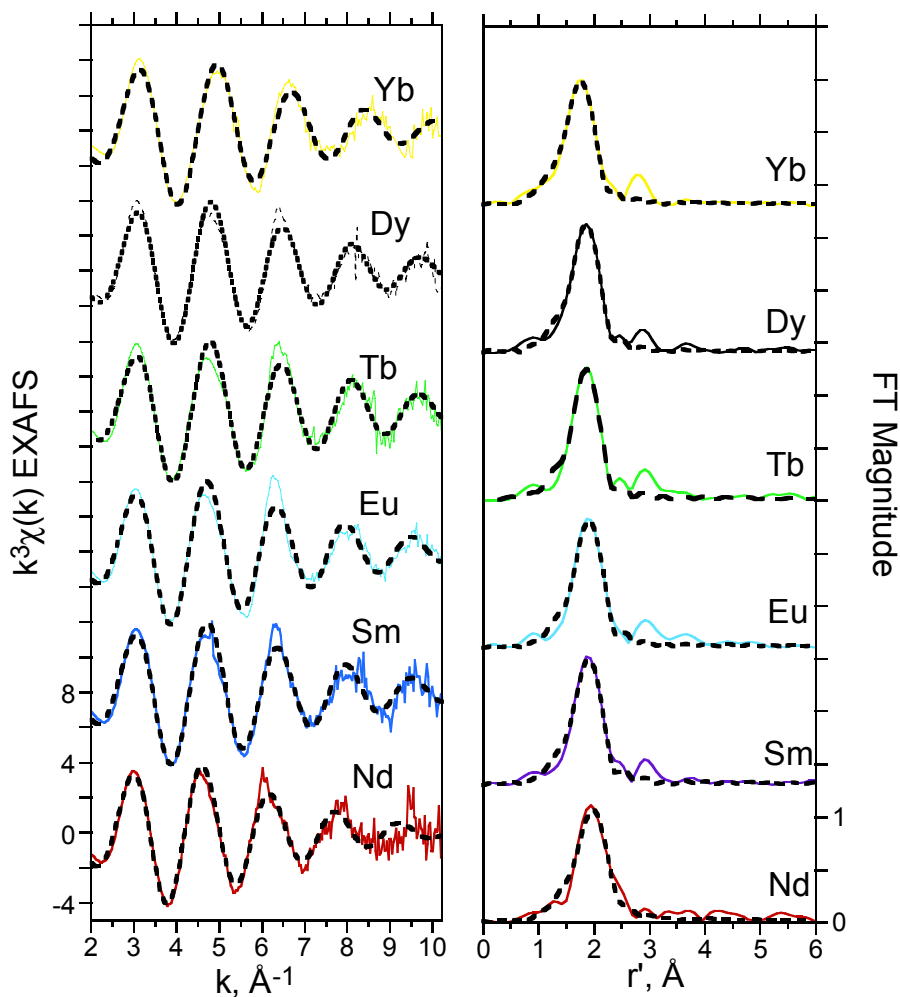


**Figure S7b.** The  $\text{Ln L}_3$ -edge  $k^3\chi(k)$  EXAFS data and corresponding FT data for the 4.3 mM solutions of  $\text{TBA}^+\text{-Ln-}\alpha\text{-1}$  in the acetonitrile electrolyte (0.1 M  $\text{TBAPF}_6$ ). The experimental data are shown as solid lines and the fits obtained by using the one O-shell model are shown as dashed lines. The metrical parameters are provided in the article itself, Tables 2 and 4.

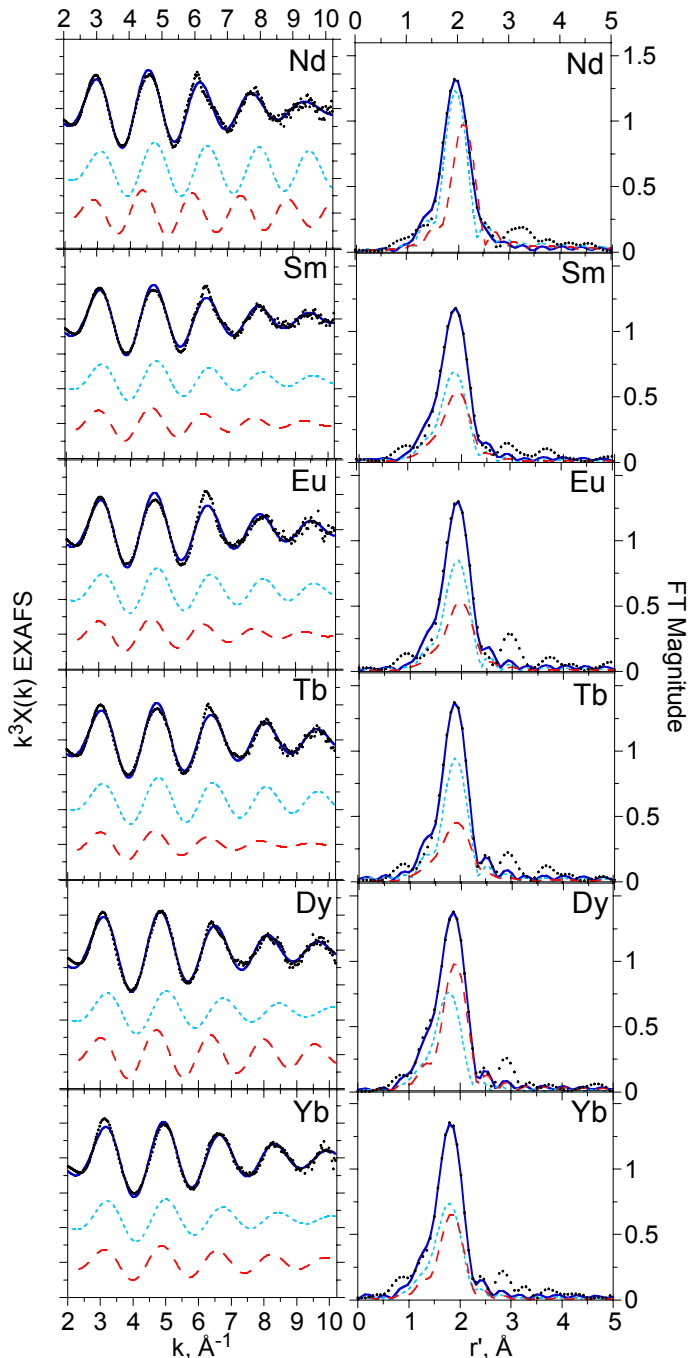


**Figure S8a.** The  $\text{Ln L}_3$ -edge  $k^3\chi(k)$  EXAFS data and corresponding FT data for the neat  $\text{TBA}^+\text{-Ln-}\alpha\text{-1}$  salts (shown with points) as well as the fits by using the 2 shell model of  $\text{O}_{\alpha-1}$  and  $\text{O}_{\text{H}_2\text{O}}$ , whose contributions are shown are teal and red dashed lines, respectively.

The composite best fits are shown as the solid blue lines, and the metrical parameters are provided in Table S4.

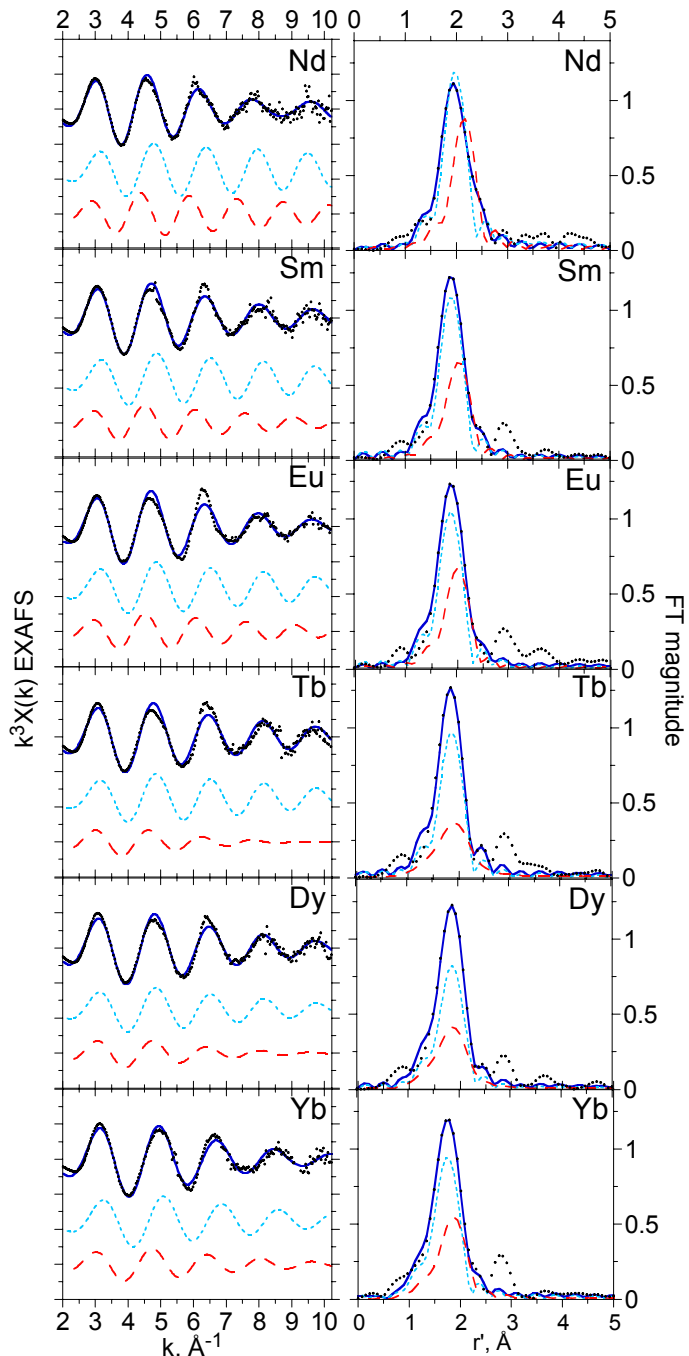


**Figure S8b.** The  $\text{Ln L}_3$ -edge  $k^3\chi(k)$  EXAFS data and corresponding FT data for the 4.3 mM solutions of  $\text{TBA}^+\text{-Ln-}\alpha\text{-1}$  (shown with points) in the acetonitrile electrolyte (0.1 M  $\text{TBAPF}_6$ ) and the fits by using the 2 shell model of  $\text{O}_{a-1}$  and  $\text{O}_{\text{H}_2\text{O}}$ , whose contributions are shown as teal and red dashed lines, respectively. The composite best fits are shown as the solid blue lines, and the metrical parameters are provided in the article, Tables 2 and 4.

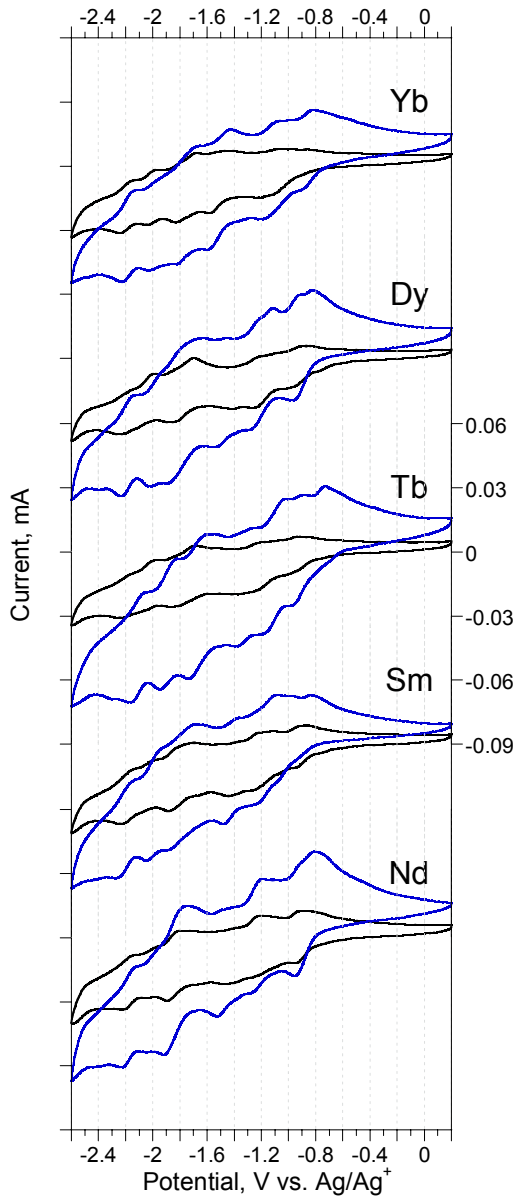


**Figure S9.** Cyclic voltammograms of 1.5 mM (black lines) and 3.5 mM (blue lines) solutions of the TBA<sup>+</sup> salts of Nd- $\alpha$ -1, Sm- $\alpha$ -1, Tb- $\alpha$ -1, Dy- $\alpha$ -1, and Yb- $\alpha$ -1 obtained with GC electrodes in dry MeCN with 0.1 M TBAPF<sub>6</sub> electrolyte at  $v = 100 \text{ mV s}^{-1}$ , starting at +0.2 V.

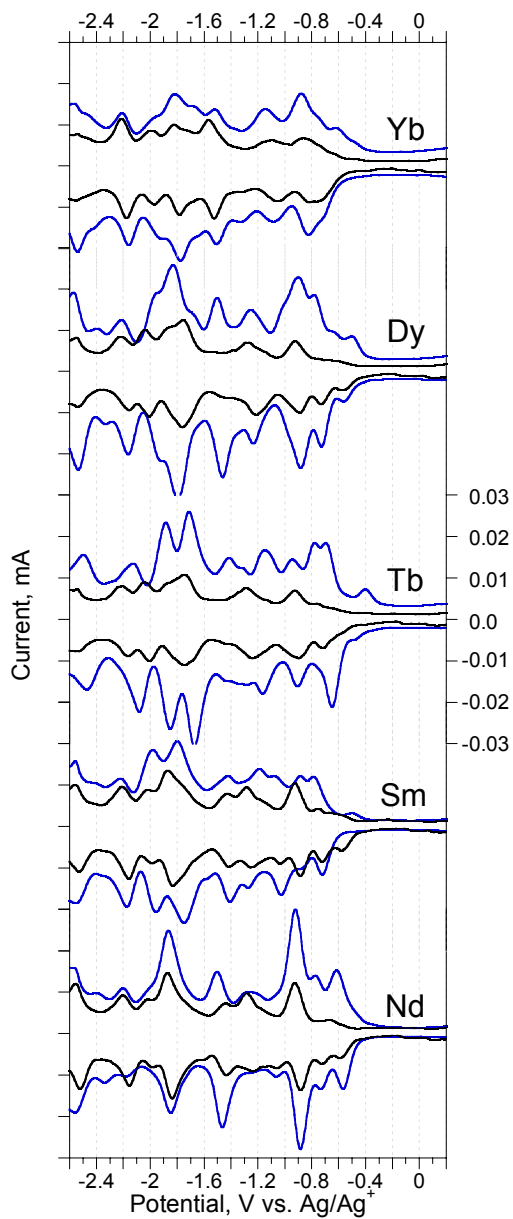


**Figure S10.** DPV data for 1.5 mM (black lines) and 3.5 mM (blue lines)  $\text{TBA}^+$  salts of Nd- $\alpha$ -1, Sm- $\alpha$ -1, Tb- $\alpha$ -1, Dy- $\alpha$ -1, and Yb- $\alpha$ -1 obtained with GC electrodes in dry MeCN with 0.1 M TBAPF<sub>6</sub> electrolyte at  $v = 20 \text{ mV s}^{-1}$  from separate scans to negative and positive electrode potentials ( $E$ ) providing the negative (initial  $E = +0.2 \text{ V} \rightarrow$  final  $E = -2.6 \text{ V}$ ) and the positive (initial  $E = -2.6 \text{ V} \rightarrow$  final  $E = +0.2 \text{ V}$ ) current responses, respectively.

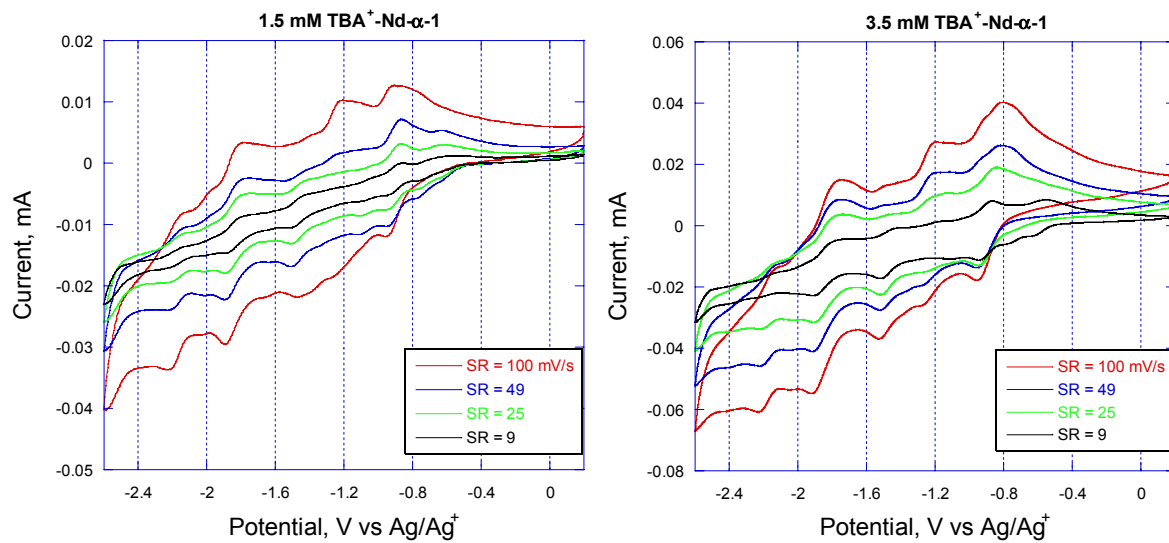


**Figure S11.** Cyclic voltammograms of 1.5 mM (left) and 3.5 mM (right) solution concentrations of the  $\text{TBA}^+$  salt of the Nd(III) complex with  $\alpha\text{-1-[P}_2\text{W}_{17}\text{O}_{61}]^{10-}$  in dry acetonitrile with 0.1 M TBAPF<sub>6</sub> electrolyte obtained with a GC electrode working electrode and different scan rates in  $\text{mV s}^{-1}$ , starting at +0.2 V.

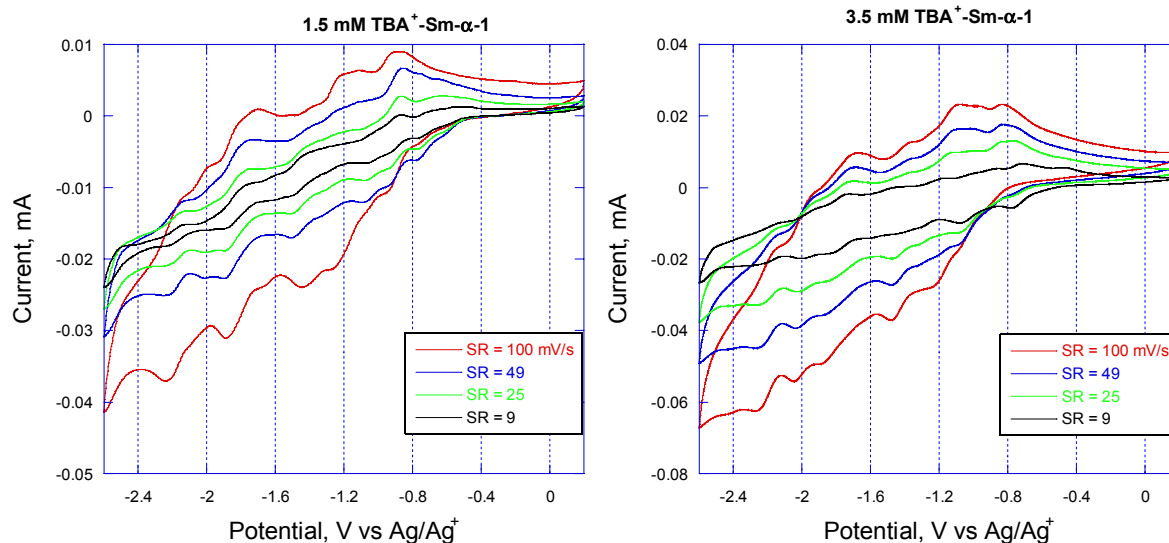


**Figure S12.** Cyclic voltammograms of 1.5 mM (left) and 3.5 mM (right) solution concentrations of the  $\text{TBA}^+$  salt of the Sm(III) complex with  $\alpha\text{-1-[P}_2\text{W}_{17}\text{O}_{61}]^{10-}$  in dry acetonitrile with 0.1 M TBAPF<sub>6</sub> electrolyte obtained with a GC electrode working electrode and different scan rates in  $\text{mV s}^{-1}$ , starting at +0.2 V.

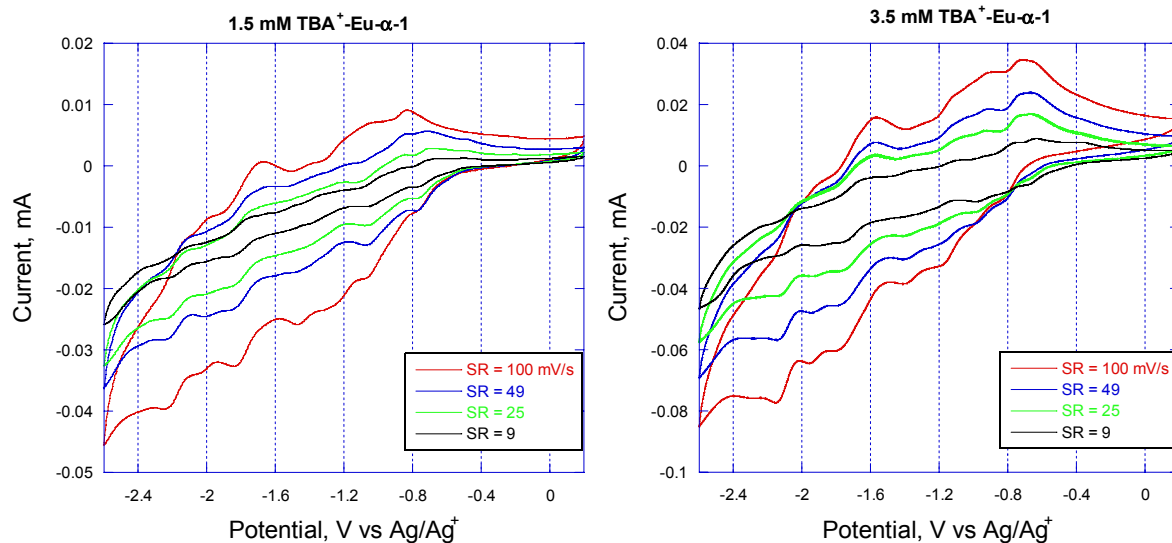


**Figure S13.** Cyclic voltammograms of 1.5 mM (left) and 3.5 mM (right) solution concentrations of the TBA<sup>+</sup> salt of the Eu(III) complex with  $\alpha$ -1-[P<sub>2</sub>W<sub>17</sub>O<sub>61</sub>]<sup>10-</sup> in dry acetonitrile with 0.1 M TBAPF<sub>6</sub> electrolyte obtained with a GC electrode working electrode and different scan rates in mV s<sup>-1</sup>, starting at +0.2 V.

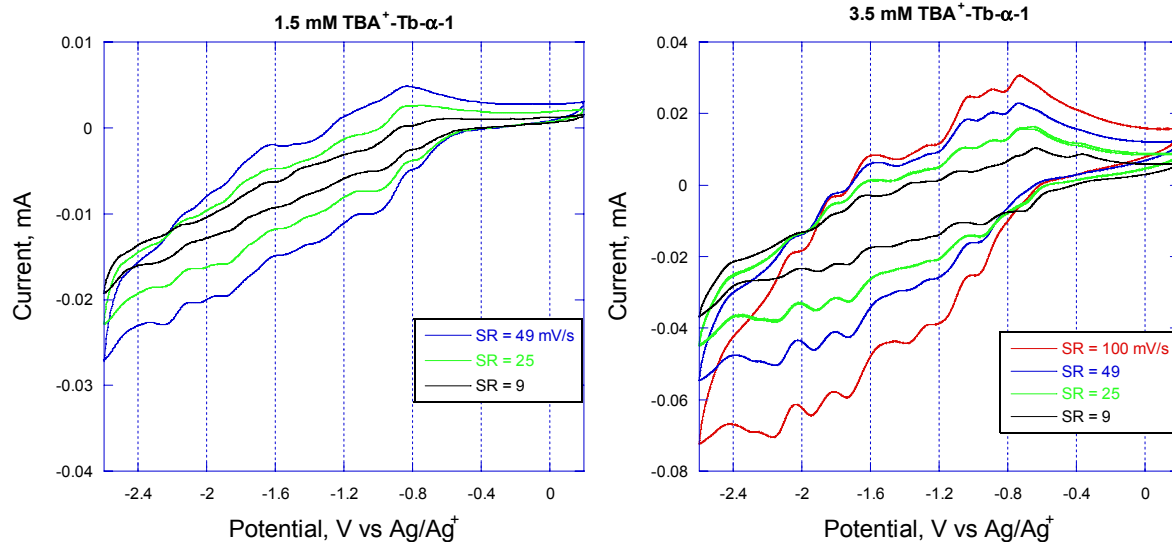


**Figure S14.** Cyclic voltammograms of 1.5 mM (left) and 3.5 mM (right) solution concentrations of the TBA<sup>+</sup> salt of the Tb(III) complex with  $\alpha$ -1-[P<sub>2</sub>W<sub>17</sub>O<sub>61</sub>]<sup>10-</sup> in dry acetonitrile with 0.1 M TBAPF<sub>6</sub> electrolyte obtained with a GC electrode working electrode and different scan rates in mV s<sup>-1</sup>, starting at +0.2 V.

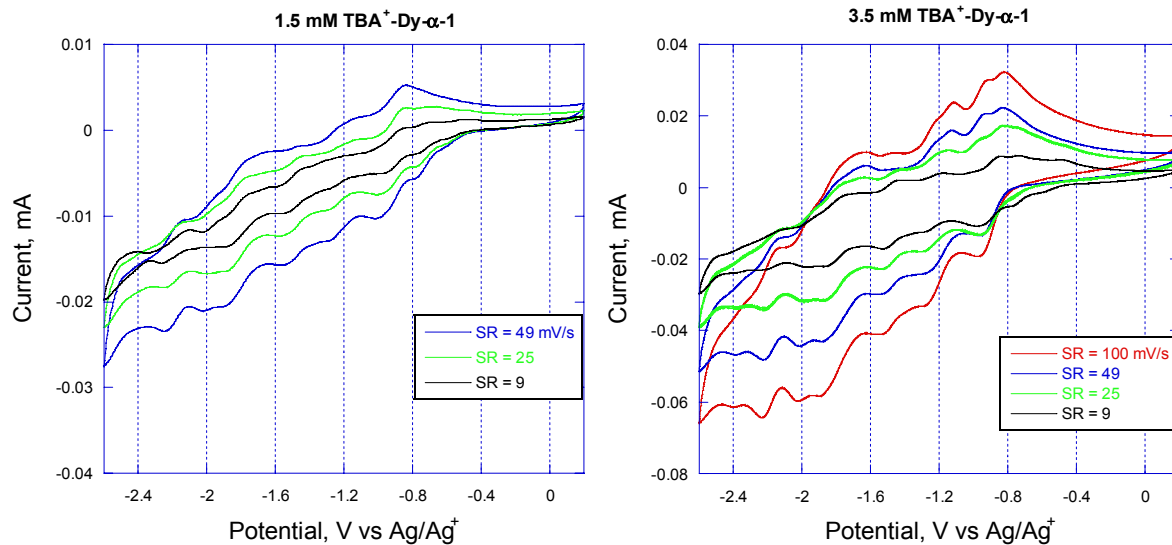


**Figure S15.** Cyclic voltammograms of  $1.5 \text{ mM}$  (left) and  $3.5 \text{ mM}$  (right) solution concentrations of the  $\text{TBA}^+$  salt of the  $\text{Dy(III)}$  complex with  $\alpha\text{-1-[P}_2\text{W}_{17}\text{O}_{61}]^{10-}$  in dry acetonitrile with  $0.1 \text{ M }$   $\text{TBAPF}_6$  electrolyte obtained with a GC electrode working electrode and different scan rates in  $\text{mV s}^{-1}$ , starting at  $+0.2 \text{ V}$ .

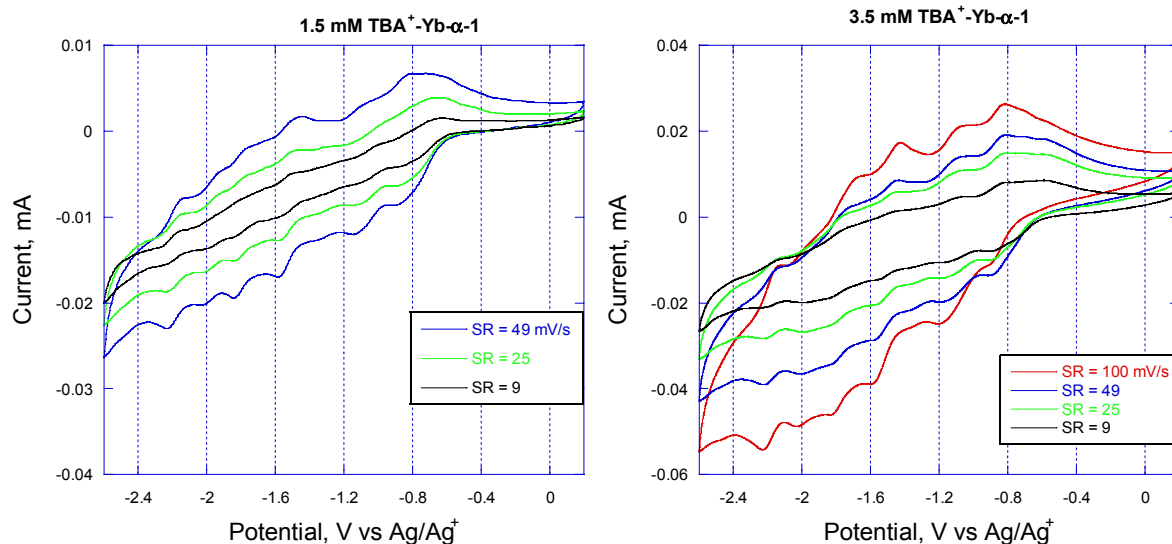


**Figure S16.** Cyclic voltammograms of  $1.5 \text{ mM}$  (left) and  $3.5 \text{ mM}$  (right) solution concentrations of the  $\text{TBA}^+$  salt of the  $\text{Yb(III)}$  complex with  $\alpha\text{-1-[P}_2\text{W}_{17}\text{O}_{61}]^{10-}$  in dry acetonitrile with  $0.1 \text{ M }$   $\text{TBAPF}_6$  electrolyte obtained with a GC electrode working electrode and different scan rates in  $\text{mV s}^{-1}$ , starting at  $+0.2 \text{ V}$ .

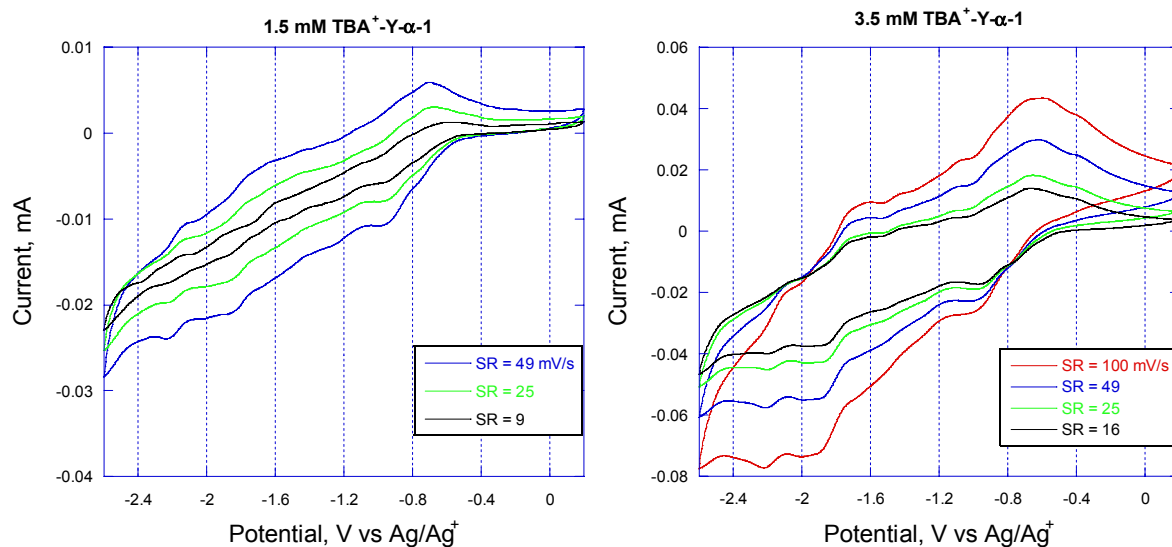


**Figure S17.** Cyclic voltammograms of 1.5 mM (left) and 3.5 mM (right) solution concentrations of the TBA<sup>+</sup> salt of the Y(III) complex with  $\alpha$ -1-[P<sub>2</sub>W<sub>17</sub>O<sub>61</sub>]<sup>10-</sup> in dry acetonitrile with 0.1 M TBAPF<sub>6</sub> electrolyte obtained with a GC electrode working electrode and different scan rates in mV s<sup>-1</sup>, starting at +0.2 V.

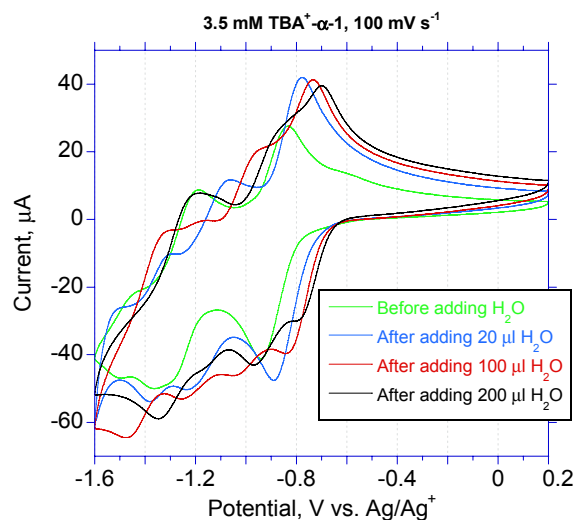


**Figure S18.** Cyclic voltammograms of the TBA<sup>+</sup> salt for a fresh 3.5 mM solution of  $\alpha$ -1-[P<sub>2</sub>W<sub>17</sub>O<sub>61</sub>]<sup>10-</sup> (lime color line) in MeCN with 0.1 M TBAPF<sub>6</sub> electrolyte and after the deliberate, successive addition of 20, 100, and 200  $\mu$ L of H<sub>2</sub>O.

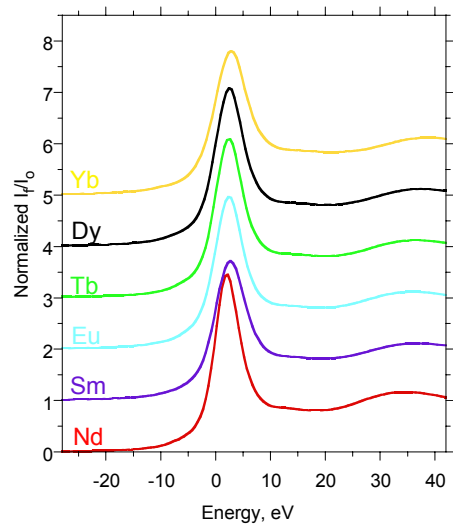


**Figure S19.** Normalized Ln L<sub>3</sub>-edge XANES,  $I_f/I_0$ , for the neat, TBA<sup>+</sup>-Ln- $\alpha$ -1 solid salts. The inflection point energies obtained from the first differential XANES are given in Table S9.

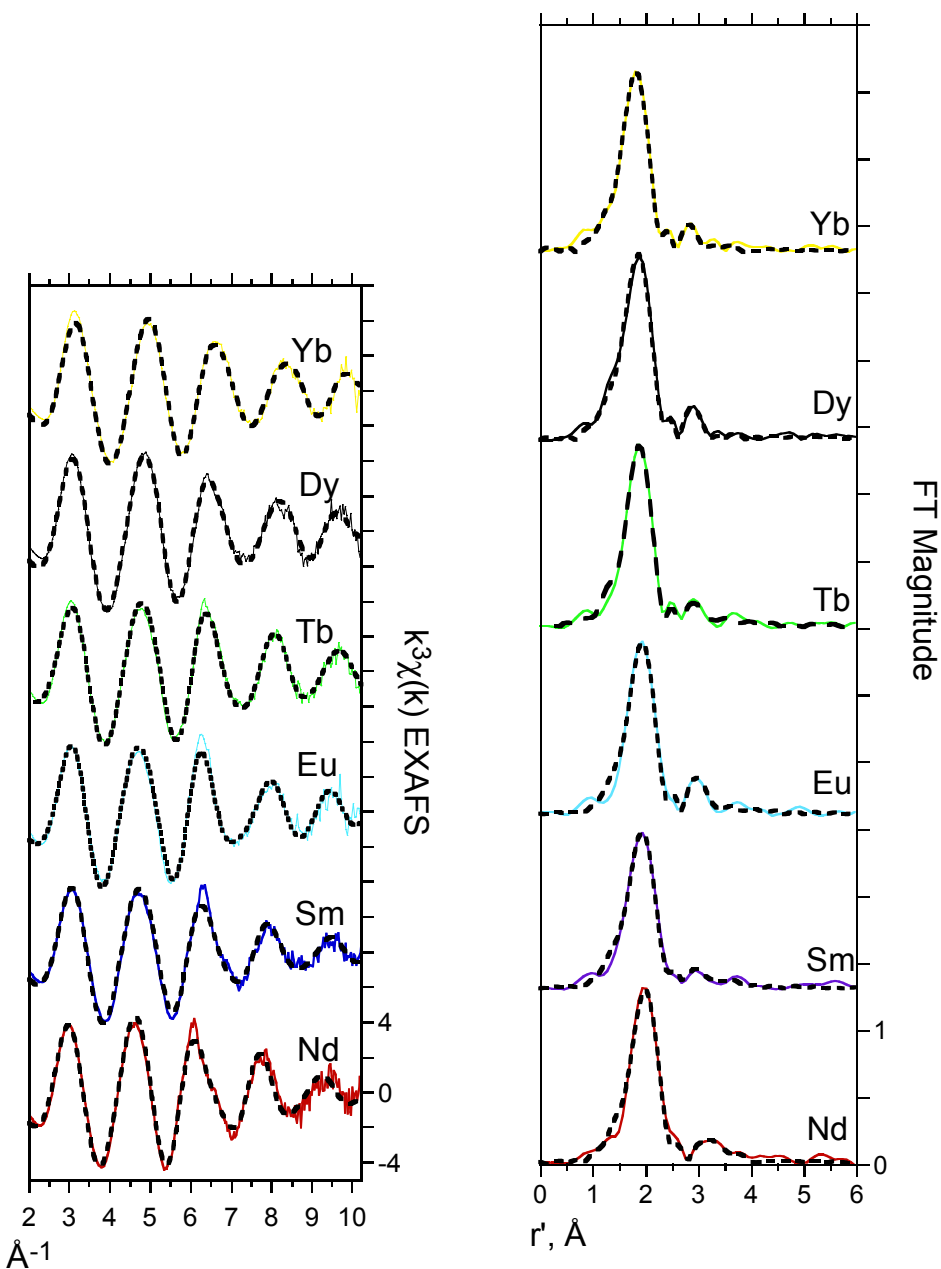


**Figure S20a.** Ln L<sub>3</sub>-edge  $k^3\chi(k)$  EXAFS data (left) and the corresponding FT data (right) for the neat TBA<sup>+</sup>-Ln- $\alpha$ -1 solid salts. The solid lines illustrate the experimental data, and the dashed lines show the fits with the multishell model, which includes Ln-O, Ln-O, and Ln-W paths. The metrical parameters are provided in Table S6.

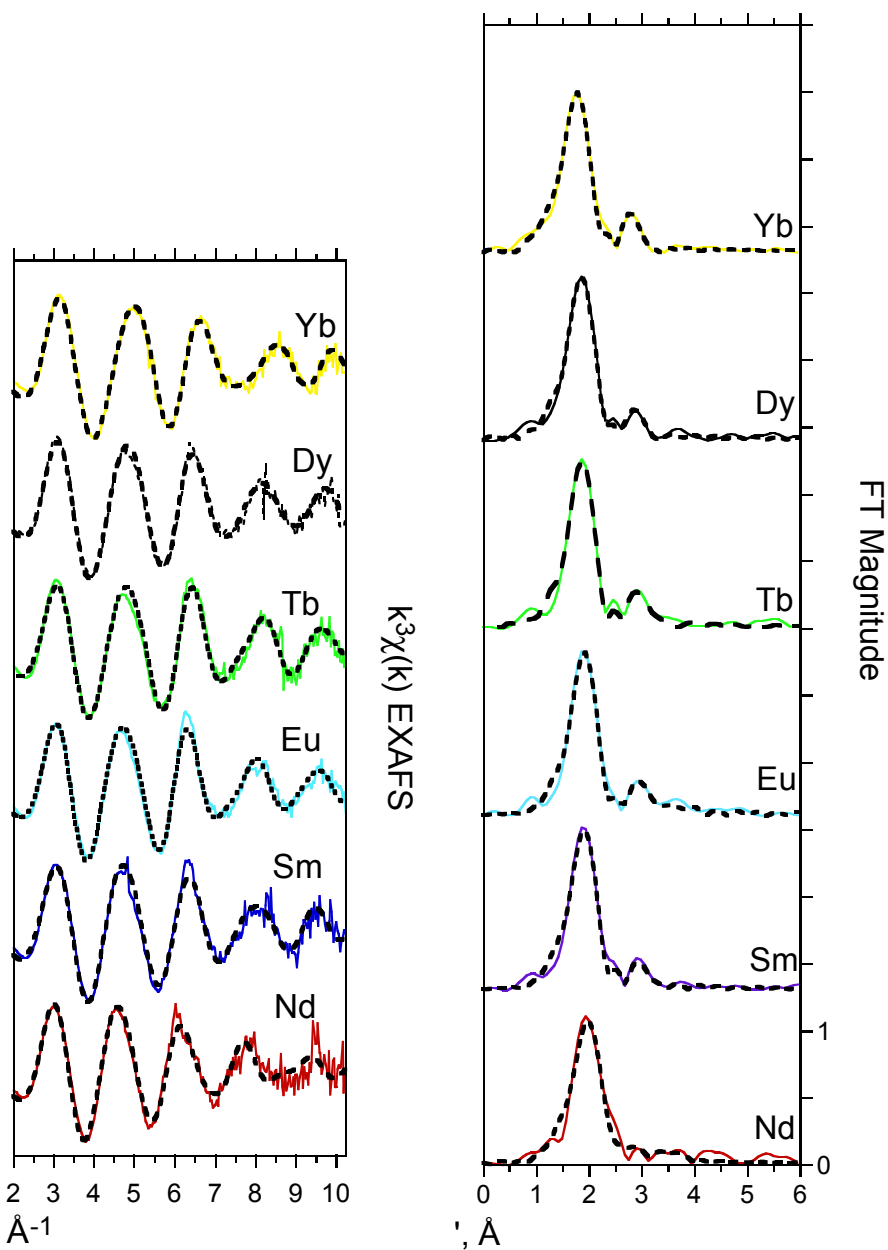


**Figure S20b.** Ln L<sub>3</sub>-edge  $k^3\chi(k)$  EXAFS data (left) and the corresponding FT data (right) for the 4.3 mM solutions of TBA<sup>+</sup>-Ln-\(\alpha\)-1 in the acetonitrile electrolyte (0.1 M TBAPF<sub>6</sub>). The solid lines illustrate the experimental data, and the dashed lines show the fits with the multishell model, which includes Ln-O, Ln-O, and Ln-W paths. The metrical parameters are provided in Table S6.

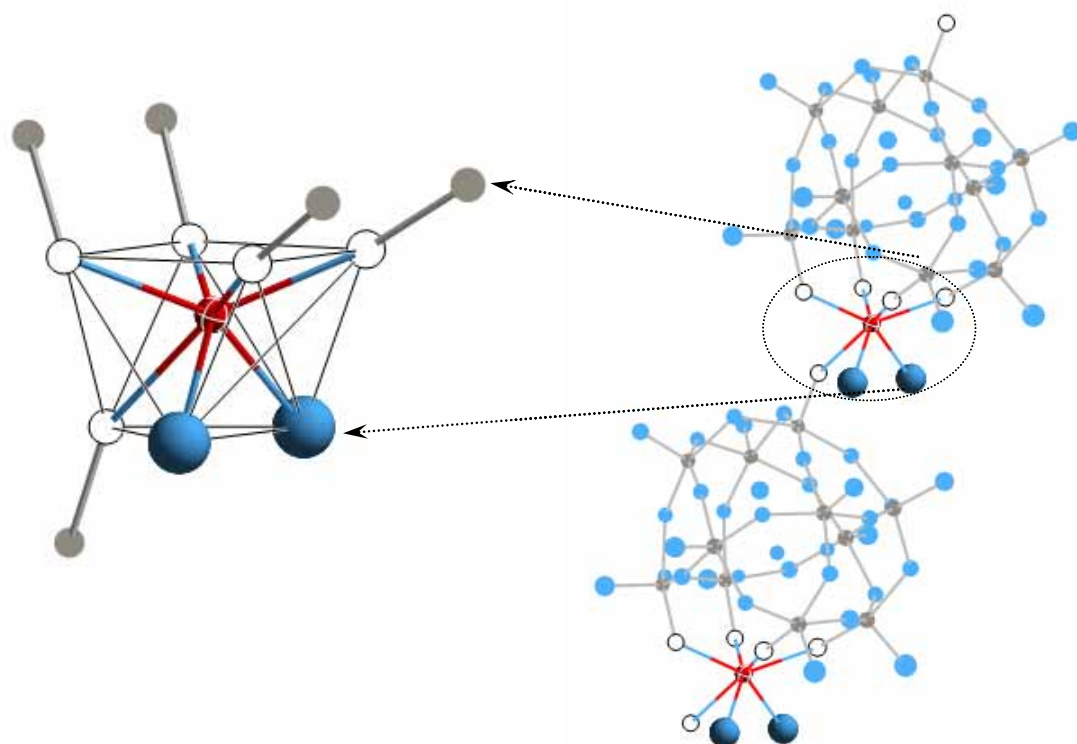


**Figure S21.** Ball and stick model of the 7 O coordination environment of Yb(III) with a capped trigonal prism geometry in  $[(\text{H}_2\text{O})_2\text{Yb}(\alpha\text{-SiW}_{11}\text{O}_{39})]^{5-}$  as the K-Cs<sub>4</sub> salt.<sup>2</sup> The red circle is the Yb ion which is connected to two terminal  $\text{O}_{\text{H}_2\text{O}}$  (blue circles) and  $\text{O}_{\alpha-1}$  atoms (open circles) bridging to W atoms (gray circles). The inset shows a fraction of the infinite linear arrangement of the molecular anions.

**Table S1.** Results from the one-O shell fits of the Ln L<sub>3</sub>-edge  $k^3\chi(k)$  EXAFS for the TBA<sup>+</sup>-Ln- $\alpha$ -1 solid salts.<sup>a</sup>

Powders	O CN <sup>b</sup>	$r$ , <sup>c</sup> Å	$\sigma^2$ , <sup>d</sup> Å <sup>2</sup>	$\Delta E_0$ , <sup>e</sup> eV
TBA <sup>+</sup> -Nd- $\alpha$ -1	9.0(7)	2.48(1)	0.012(1)	0.6
TBA <sup>+</sup> -Sm- $\alpha$ -1	7.8(5)	2.42(1)	0.013(1)	0.7
TBA <sup>+</sup> -Eu- $\alpha$ -1	7.6(7)	2.41(1)	0.011(1)	2.1
TBA <sup>+</sup> -Tb- $\alpha$ -1	7.4(5)	2.36(1)	0.010(1)	-0.9
TBA <sup>+</sup> -Dy- $\alpha$ -1	8.4(5)	2.33(1)	0.012(1)	-1.0
TBA <sup>+</sup> -Yb- $\alpha$ -1	6.9(4)	2.27(1)	0.011(1)	1.0

<sup>a</sup> The numbers in the parentheses represent the estimated standard deviations ( $3\sigma$ ) obtained from the least-squares fits. <sup>b</sup> Coordination number. <sup>c</sup> Interatomic distance. <sup>d</sup> The Debye-Waller factor, the root-mean-square deviation of the average Ln-O bond length. <sup>e</sup> The energy difference between the experimental and theoretical values of  $E_0$ .

**Table S2.** Results from the one-O shell of the Ln L<sub>3</sub>-edge  $k^3\chi(k)$  EXAFS of the aqueous solutions of 4.3 mM K<sup>+</sup>-Ln- $\alpha$ -1 salts. The parameter definitions are given in the footnotes to Table S1.

Solution	O CN	$r$ , Å	$\sigma^2$ , Å <sup>2</sup>	$\Delta E_0$ , eV
K <sup>+</sup> -Nd- $\alpha$ -1	8.8(15)	2.45(2)	0.013(3)	0.7
K <sup>+</sup> -Sm- $\alpha$ -1	8.8(9)	2.40(1)	0.012(2)	0.2
K <sup>+</sup> -Eu- $\alpha$ -1	7.6(9)	2.38(1)	0.009(2)	0.6
K <sup>+</sup> -Tb- $\alpha$ -1	8.1(6)	2.35(1)	0.010(1)	0.9
K <sup>+</sup> -Dy- $\alpha$ -1	8.6(9)	2.33(1)	0.011(2)	-1.5
K <sup>+</sup> -Yb- $\alpha$ -1	7.3(7)	2.26(1)	0.010(1)	0.8

**Table S3.** Results from the one-O shell fits of the Ln L<sub>3</sub>-edge  $k^3\chi(k)$  EXAFS of the TBA<sup>+</sup>-Ln- $\alpha$ -1 solid salts and their 4.3 mM solutions in the acetonitrile electrolyte (0.1 M TBAPF<sub>6</sub>). Fit results take the Ln-O pair distribution asymmetry into consideration by including the third cumulant  $\sigma'$  and the fourth cumulant  $\sigma''$ . Other parameter definitions are given in the footnotes to Table S1.

Sample	O CN	r, Å	$\sigma^2$ , Å <sup>2</sup>	$\sigma'$	$\sigma''$	$\Delta E_0$
TBA <sup>+</sup> -Nd- $\alpha$ -1 powder	8.0(4)	2.48(1)	0.006 (1)	0.0001(1)	-0.0002(1)	2.9
TBA <sup>+</sup> -Nd- $\alpha$ -1 solution	7.6(2)	2.53(1)	0.006 (1)	0.0016(1)	-0.0004(1)	4.6
TBA <sup>+</sup> -Sm- $\alpha$ -1 powder	9.0(2)	2.44(1)	0.014 (1)	0.0004(1)	0.00005(1)	4.0
TBA <sup>+</sup> -Sm- $\alpha$ -1 solution	8.2(1)	2.43(1)	0.011 (1)	0.0007(1)	-0.00006(1)	3.4
TBA <sup>+</sup> -Eu- $\alpha$ -1 powder	7.2(1)	2.46(1)	0.007 (1)	0.001(1)	-0.00014(1)	6.2
TBA <sup>+</sup> -Eu- $\alpha$ -1 solution	7.1(1)	2.46(1)	0.007 (1)	0.001(1)	-0.00015(2)	6.0
TBA <sup>+</sup> -Tb- $\alpha$ -1 powder	7.8(1)	2.38(1)	0.009 (1)	0.0002(1)	-0.000007(10)	2.0
TBA <sup>+</sup> -Tb- $\alpha$ -1 solution	8.1(1)	2.38(1)	0.012 (1)	0.0006(1)	0.00005(1)	2.0
TBA <sup>+</sup> -Dy- $\alpha$ -1 powder	8.8(2)	2.35(1)	0.012 (1)	0.000003(1)	0.00002(1)	1.7
TBA <sup>+</sup> -Dy- $\alpha$ -1 solution	8.7(2)	2.38(1)	0.015 (1)	0.0007(1)	0.00012(1)	2.8
TBA <sup>+</sup> -Yb- $\alpha$ -1 powder	7.1(1)	2.29(1)	0.010 (1)	0.0003(1)	0.00002(1)	3.9
TBA <sup>+</sup> -Yb- $\alpha$ -1 solution	7.3(1)	2.32(1)	0.013 (1)	0.0015(1)	0.00008(1)	4.7

**Table S4.** Results from the two-O shell ( $O_{\alpha-1}$  and  $O_{H_2O}$ ) curve-fitting of the Ln L<sub>3</sub>-edge  $k^3\chi(k)$  EXAFS of the TBA<sup>+</sup>-Ln- $\alpha$ -1 solid salts. The parameter definitions are given in the footnotes to Table S1.

Powders	Shell	CN	$r, \text{\AA}$	$\sigma^2, \text{\AA}^2$	$\Delta E_0, \text{eV}$
TBA <sup>+</sup> -Nd- $\alpha$ -1	$O_{\alpha-1}$	4	2.42(1)	0.003(2)	1.4
	$O_{H_2O}$	4.3(8)	2.58(2)	0.005(3)	/ <sup>a</sup>
TBA <sup>+</sup> -Sm- $\alpha$ -1	$O_{\alpha-1}$	4	2.39(20)	0.010(6)	0.8
	$O_{H_2O}$	3.9(8)	2.45(24)	0.013(29)	/
TBA <sup>+</sup> -Eu- $\alpha$ -1	$O_{\alpha-1}$	4	2.38(8)	0.008(3)	2.4
	$O_{H_2O}$	3.8(11)	2.46(11)	0.013(20)	/
TBA <sup>+</sup> -Tb- $\alpha$ -1	$O_{\alpha-1}$	4	2.35(2)	0.006(2)	-0.4
	$O_{H_2O}$	3.8(10)	2.39(5)	0.017(10)	/
TBA <sup>+</sup> -Dy- $\alpha$ -1	$O_{\alpha-1}$	4	2.26(2)	0.010(6)	-1.9
	$O_{H_2O}$	4.4(7)	2.37(3)	0.006(3)	/
TBA <sup>+</sup> -Yb- $\alpha$ -1	$O_{\alpha-1}$	4	2.25(9)	0.012(15)	0.7
	$O_{H_2O}$	3.0(7)	2.30(13)	0.008(4)	/

<sup>a</sup> The / notation indicates that the parameter was fixed to the value in the column above.

**Table S5.** Results from the two-O shell ( $O_{\alpha-1}$  and  $O_{H_2O}$ ) curve-fitting of the Ln L<sub>3</sub>-edge  $k^3\chi(k)$  EXAFS for the 4.3 mM K<sup>+</sup>-Ln- $\alpha$ -1 aqueous solutions. The parameter definitions are given in the footnotes to Table S1.

Solution	Shell	CN	$r, \text{\AA}$	$\sigma^2, \text{\AA}^2$	$\Delta E_0, \text{eV}$
K <sup>+</sup> -Nd- $\alpha$ -1	$O_{\alpha-1}$	4	2.40(2)	0.002(4)	1.8
	$O_{H_2O}$	4.4(16)	2.56(3)	0.005(7)	/ <sup>a</sup>
K <sup>+</sup> -Sm- $\alpha$ -1	$O_{\alpha-1}$	4	2.34(2)	0.004(4)	0.7
	$O_{H_2O}$	4.3(10)	2.48(3)	0.005(6)	/
K <sup>+</sup> -Eu- $\alpha$ -1	$O_{\alpha-1}$	4	2.36(3)	0.004(3)	2.2
	$O_{H_2O}$	4.4(17)	2.48(5)	0.013(14)	/
K <sup>+</sup> -Tb- $\alpha$ -1	$O_{\alpha-1}$	4	2.27(4)	0.007(8)	-2.3
	$O_{H_2O}$	4.8(15)	2.39(4)	0.008(8)	/
K <sup>+</sup> -Dy- $\alpha$ -1	$O_{\alpha-1}$	4	2.24(6)	0.016(13)	-3.1
	$O_{H_2O}$	4.3(16)	2.35(3)	0.007(3)	/
K <sup>+</sup> -Yb- $\alpha$ -1	$O_{\alpha-1}$	4	2.24(5)	0.009(15)	0.7
	$O_{H_2O}$	3.3(10)	2.29(7)	0.009(22)	/

<sup>a</sup> The / notation indicates that the parameter was fixed to the value in the column above.

**Table S6.** Parameters from curve-fitting analysis (multi-shell fit) of the Ln L<sub>3</sub>-edge  $k^3\chi(k)$  EXAFS of Figure S20. The parameters are defined in the footnotes to Table S1.

Sample	Shell	CN	$r$ , Å	$\sigma^2$ , Å <sup>2</sup>	$\Delta E_0$ , eV
TBA <sup>+</sup> -Nd- $\alpha$ -1 Powder	Nd-O	9.0(6)	2.48(1)	0.012(1)	0.6
	Nd-O	1	3.63(7)	0.007(10)	/ <sup>a</sup>
	Nd-W	4	3.87(4)	0.018(5)	/
TBA <sup>+</sup> -Sm- $\alpha$ -1 Powder	Sm-O	7.7(5)	2.42(1)	0.013(1)	0.6
	Sm-O	1	3.42(6)	0.010(9)	/
	Sm-W	4	3.75(4)	0.020(5)	/
TBA <sup>+</sup> -Eu- $\alpha$ -1 Powder	Eu-O	7.7(5)	2.40(1)	0.011(1)	1.8
	Eu-O	1	3.44(3)	0.0005(11)	/
	Eu-W	4	3.71(4)	0.019(5)	/
TBA <sup>+</sup> -Tb- $\alpha$ -1 Powder	Tb-O	7.4(4)	2.36(1)	0.009(1)	-1.0
	Tb-O	1	3.34(6)	0.010(9)	/
	Tb-W	4	3.63(3)	0.019(4)	/
TBA <sup>+</sup> -Dy- $\alpha$ -1 Powder	Dy-O	8.5(5)	2.33(1)	0.012(1)	-1.2
	Dy-O	1	3.38(2)	0.0003(8)	/
	Dy-W	4	3.69(6)	0.028(11)	/
TBA <sup>+</sup> -Yb- $\alpha$ -1 Powder	Yb-O	7.0(4)	2.27(1)	0.011(1)	0.8
	Yb-O	1	3.30(3)	0.002(3)	/
	Yb-W	4	3.66(5)	0.025(8)	/

<sup>a</sup> The / notation indicates that the parameter was fixed to the value in the column above.

Sample	Shell	CN	$r, \text{\AA}$	$\sigma^2, \text{\AA}^2$	$\Delta E_0, \text{eV}$
TBA <sup>+</sup> -Nd- $\alpha$ -1 Solution	Nd-O	8.7(10)	2.48(1)	0.015(2)	0.7
	Nd-O	1	3.41(6)	0.006(8)	/
	Nd-W	4	3.82(4)	0.018(6)	/
TBA <sup>+</sup> -Sm- $\alpha$ -1 Solution	Sm-O	7.6(6)	2.40(1)	0.012(1)	-0.4
	Sm-O	1	3.41(3)	0.0005(11)	/
	Sm-W	4	3.4(3)	0.05(8)	/
TBA <sup>+</sup> -Eu- $\alpha$ -1 Solution	Eu-O	7.4(5)	2.39(1)	0.012(1)	1.4
	Eu-O	1	3.39(3)	0.002(4)	/
	Eu-W	4	3.66(3)	0.016(4)	/
TBA <sup>+</sup> -Tb- $\alpha$ -1 Solution	Tb-O	7.1(6)	2.35(1)	0.01(1)	-1.1
	Tb-O	1	3.35(4)	0.002(5)	/
	Tb-W	4	3.54(4)	0.019(5)	/
TBA <sup>+</sup> -Dy- $\alpha$ -1 Solution	Dy-O	7.4(5)	2.34(1)	0.012(1)	-0.8
	Dy-O	1	3.32(3)	0.002(3)	/
	Dy-W	4	3.60(5)	0.023(7)	/
TBA <sup>+</sup> -Yb- $\alpha$ -1 Solution	Yb-O	7.3(5)	2.25(1)	0.013(1)	-0.859
	Yb-O	1	3.26(2)	-0.001(2)	/
	Yb-W	4	3.50(6)	0.027(9)	/

**Notes for Table S7:**

The single-shell curve-fitting results for the Ln L<sub>3</sub>-edge  $k^3\chi(k)$  EXAFS presented in Tables 2 and 4 of the article text provide only average Ln-O distances for the Ln- $\alpha$ -1 complexes. Nevertheless, the two sets of individual distances, which are attributed to the 4 bridging O atoms from the  $\alpha$ -1 ligand ( $O_{\alpha-1}$ ) and n = 3–5 terminal O atoms from water molecules ( $O_{H_2O}$ ) coordinated to the Ln(III) ions, can be estimated from the EXAFS-determined Debye-Waller factors,  $\sigma^2$ , which provide a measure of the total spread ( $\delta r$ ) in the Ln-O distances, for the one-O shell fits. Through use of a procedure outlined previously,<sup>3,4</sup> it was possible to determine the mean Ln- $O_{H_2O}$  and Ln- $O_{\alpha-1}$  interatomic distances,  $r_n$  and  $r_m$ , respectively. The results are summarized here in Tables S7a and S7b, where we have assumed that the four Ln- $O_{\alpha-1}$  distances are shorter than all the Ln- $O_{H_2O}$  ones (exactly as obtains in the crystal structures),<sup>5–7</sup> and assuming integer values for the hydration numbers, n, based upon the best fit CNs. The results are in excellent correspondence with the two sets of individual distances obtained from the two-shell model, presented in Tables 2 and 4 of the article text.

**Table S7a.** Results for the acetonitrile solutions (4.3 mM) of the TBA<sup>+</sup>-Ln- $\alpha$ -1 salts.

Solution	$\sigma_{vib}^b$	$\sigma_{exp}^c$	$\sigma_{cal}^d$	n <sup>a</sup>	$\delta r^e$	$r_{exp}^f$	$r_{m, cal}^g$	$r_{n, cal}^g$	$r_{m, exp}^h$	$r_{n, exp}^h$
TBA <sup>+</sup> -Nd- $\alpha$ -1	0.074	0.126	0.103	5	0.144	2.48	2.40	2.54	2.43	2.60
TBA <sup>+</sup> -Sm- $\alpha$ -1	0.072	0.110	0.102	4	0.143	2.40	2.33	2.47	2.36	2.51
TBA <sup>+</sup> -Eu- $\alpha$ -1	na	0.110	na	4	0.143	2.40	2.33	2.47	2.35	2.49
TBA <sup>+</sup> -Tb- $\alpha$ -1	0.070	0.100	0.100	4	0.143	2.35	2.28	2.42	2.34	2.42
TBA <sup>+</sup> -Dy- $\alpha$ -1	0.069	0.110	0.099	4	0.143	2.34	2.27	2.41	2.33	2.37
TBA <sup>+</sup> -Yb- $\alpha$ -1	0.066	0.134	0.097	3	0.144	2.25	2.19	2.33	2.21	2.34

**Table S7b.** Results for the solid TBA<sup>+</sup>-Ln- $\alpha$ -1 salts.

Powders	$\sigma_{\text{vib}}^b$	$\sigma_{\text{exp}}^c$	$\sigma_{\text{cal}}^d$	n <sup>a</sup>	$\delta r^e$	$r_{\text{exp}}^f$	$r_m, \text{cal}^g$	$r_n, \text{cal}^g$	$r_m, \text{exp}^h$	$r_n, \text{exp}^h$
TBA <sup>+</sup> -Nd- $\alpha$ -1	0.074	0.126	0.103	5	0.144	2.48	2.40	2.54	2.42	2.58
TBA <sup>+</sup> -Sm- $\alpha$ -1	0.072	0.110	0.102	4	0.143	2.42	2.35	2.49	2.39	2.45
TBA <sup>+</sup> -Eu- $\alpha$ -1	na <sup>i</sup>	0.110	na	4	0.143	2.41	2.34	2.48	2.38	2.46
TBA <sup>+</sup> -Tb- $\alpha$ -1	0.070	0.100	0.100	4	0.143	2.36	2.29	2.43	2.35	2.39
TBA <sup>+</sup> -Dy- $\alpha$ -1	0.069	0.110	0.099	4	0.143	2.33	2.26	2.40	2.26	2.37
TBA <sup>+</sup> -Yb- $\alpha$ -1	0.066	0.114	0.097	3	0.144	2.27	2.21	2.35	2.25	2.30

<sup>a</sup> Value of n was obtained as the best integer CN for O<sub>H<sub>2</sub>O</sub> from the two O-shell fits; m was the fixed CN (4) for O <sub>$\alpha$ -1</sub>, which accounts for the tetradeinate ligation of Ln with the  $\alpha$ -1 ligand. <sup>b</sup> The vibrational contribution to the Debye-Waller factor,  $\sigma_{\text{vib}}$ , is calculated according to  $\sigma_{\text{vib}} = 3.151 \times 10^{-3}[(v/K) \coth(y/2)]^{1/2}$ , where  $y = 1.441(v/T)$ , the vibrational frequency, v, and the stretching force constant, K, are from Mink et al.,<sup>8</sup> and T is equal to 298 K. <sup>c</sup> The refined Debye-Waller factors from the single O-shell fitting model. <sup>d</sup>

Calculated according to  $\sigma_{\text{cal}} = (\sigma_{\text{vib}}^2 + \sigma_{\text{stat}}^2)^{1/2}$ , where  $\sigma_{\text{stat}}^2 = 0.0051 \text{ \AA}^2$  was calculated from the crystal structure of K<sup>+</sup>-Lu- $\alpha$ -1,<sup>6</sup> according to  $[\sum_{i=1}^N (r_i - r)^2 / N]^{1/2}$ , where r is the mean crystallographic value (2.355 Å) of N = 8 distances. <sup>e</sup>  $\delta r$  is calculated from  $\delta r = \sigma_{\text{stat}}(m + n)/(mn)^{1/2}$ . <sup>f</sup> The refined, average Ln-O interatomic distances from the single O-shell fitting model. <sup>g</sup> Calculated according to  $r_m = r - n\delta_r/(m + n)$ ,  $r_n = r + m\delta_r/(m + n)$ . <sup>h</sup>

Interatomic distance from the two O-shell fits. <sup>i</sup> Not available.

**Table S8.** Statistical information— $\chi^2$  is the goodness-of-fit and v is the number of degrees of freedom of the fit—obtained from fitting with the one-O-shell (4 parameter) model (A) and the two-O-shell (6 parameter) model (C) to the data of the  $\text{TBA}^+$ -Ln- $\alpha$ -1 salts (powders) and their 4.3 mM solutions in the acetonitrile electrolyte (0.1 M TBAPF<sub>6</sub>). The  $F_\chi$  test was applied in the manner of Lukens et al.<sup>9</sup>, where # ind. points =  $2(r_{\max} - r_{\min})(k_{\max} - k_{\min})/\pi + 2 = 2(2.6 - 1.0)\text{\AA}(10.2 - 2.0)(\text{\AA}^{-1})/\pi + 2$ ; v = # ind. Points - # params;  $F_\chi = v_{(C)}[\chi^2_{(A)} - \chi^2_{(C)}]/b\chi^2_{(C)}$ ; P( $F_\chi$ , b, v) comes from function FDIST in Microsoft Excel.

1.  $\text{TBA}^+$ -Nd- $\alpha$ -1 Powder:

	Model A	Model C
# params	4	6
# ind. points	10	10
b	2	-
v	6	4
$\chi^2$	975	360
$\chi^2/v$	163	<u>90</u>
$F_\chi$	3.4	
P( $F_\chi$ , b, v)	0.103	

2.  $\text{TBA}^+$ -Sm- $\alpha$ -1 Powder:

	Model A	Model C
# params	4	6
# ind. points	10	10
b	2	-
v	6	4
$\chi^2$	897	27.8
$\chi^2/v$	150	<u>6.95</u>
$F_\chi$	62.5	
P( $F_\chi$ , b, v)	0.000096	

3.  $\text{TBA}^+$ -Eu- $\alpha$ -1 Powder:

	Model A	Model C
# params	4	6
# ind. points	10	10
b	2	-
v	6	4
$\chi^2$	18962	726.1
$\chi^2/v$	3160	<u>182</u>
$F_\chi$	50.2	
P( $F_\chi$ , b, v)	0.00018	

4. TBA<sup>+</sup>-Tb- $\alpha$ -1 Powder:

	Model A	Model C
# params	4	6
# ind. points	10	10
b	2	-
v	6	4
$\chi^2$	1746	287.8
$\chi^2/v$	291	<u>71.95</u>
$F_\chi$	10.13	
$P(F_\chi, b, v)$	0.0119	

5. TBA<sup>+</sup>-Dy- $\alpha$ -1 Powder:

	Model A	Model C
# params	4	6
# ind. points	10	10
b	2	-
v	6	4
$\chi^2$	1872	286.5
$\chi^2/v$	312	<u>71.6</u>
$F_\chi$	11.07	
$P(F_\chi, b, v)$	0.0097	

6. TBA<sup>+</sup>-Yb- $\alpha$ -1 Powder:

	Model A	Model C
# params	4	6
# ind. points	10	10
b	2	-
v	6	4
$\chi^2$	2394	204.3
$\chi^2/v$	399	<u>51.1</u>
$F_\chi$	21.4	
$P(F_\chi, b, v)$	0.0019	

7. TBA<sup>+</sup>-Nd- $\alpha$ -1 Solution:

	Model A	Model C
# params	4	6
# ind. points	10	10
b	2	-
v	6	4
$\chi^2$	23082	5164
$\chi^2/v$	3847	<u>1291</u>
$F_\chi$	6.94	
$P(F_\chi, b, v)$	0.0275	

8. TBA<sup>+</sup>-Sm- $\alpha$ -1 Solution:

	Model A	Model C
# params	4	6
# ind. points	10	10
b	2	-
v	6	4
$\chi^2$	78642	6004
$\chi^2/v$	13107	<u>1501</u>
$F_\chi$	24.2	
$P(F_\chi, b, v)$	0.0013	

9. TBA<sup>+</sup>-Eu- $\alpha$ -1 Solution:

	Model A	Model C
# params	4	6
# ind. points	10	10
b	2	-
v	6	4
$\chi^2$	13999	587.5
$\chi^2/v$	2333	<u>147</u>
$F_\chi$	45.7	
$P(F_\chi, b, v)$	0.00023	

10. TBA<sup>+</sup>-Tb- $\alpha$ -1 Solution:

	Model A	Model C
# params	4	6
# ind. points	10	10
b	2	-
v	6	4
$\chi^2$	9956	80.1
$\chi^2/v$	1659	<u>20</u>
$F_\chi$	247	
$P(F_\chi, b, v)$	$1.7 \times 10^{-6}$	

11. TBA<sup>+</sup>-Dy- $\alpha$ -1 Solution:

	Model A	Model C
# params	4	6
# ind. points	10	10
b	2	-
v	6	4
$\chi^2$	13546	73.1
$\chi^2/v$	2258	<u>18</u>
$F_\chi$	369	
$P(F_\chi, b, v)$	$5.2 \times 10^{-7}$	

12. TBA<sup>+</sup>-Yb- $\alpha$ -1 Solution:

	Model A	Model C
# params	4	6
# ind. points	10	10
b	2	-
v	6	4
$\chi^2$	31189	97.2
$\chi^2/v$	5198	<u>24.3</u>
$F_\chi$	640	
$P(F_\chi, b, v)$	$1.0 \times 10^{-7}$	

**Table S9.** Results from the curve-fitting analyses of the normalized Ln L<sub>3</sub>-edge XANES of the neat powders of the TBA<sup>+</sup>-Ln- $\alpha$ -1 solid salts using XANES-Fit in WinXAS with a psedo-Voight line shape to model the edge resonance and an arctangent function to model the edge jump.

Powders	Ln edge resonances				Edge steps				ip, <sup>a</sup> eV
	Height	Position	FWHM	Area	Height	Position	FWHM		
TBA <sup>+</sup> -Nd- $\alpha$ -1	3.096	2.09	5.57	20.981	1.009	5.07	14.21		6213.7
TBA <sup>+</sup> -Sm- $\alpha$ -1	2.398	2.65	6.89	19.510	1.023	6.86	17.14		6720.0
TBA <sup>+</sup> -Eu- $\alpha$ -1	2.651	2.39	6.36	20.637	1.026	7.14	17.71		6980.6
TBA <sup>+</sup> -Tb- $\alpha$ -1	2.780	2.37	6.17	21.039	0.995	6.14	15.85		7518.4
TBA <sup>+</sup> -Dy- $\alpha$ -1	2.771	2.46	6.35	21.714	0.969	6.13	15.39		7795.2
TBA <sup>+</sup> -Yb- $\alpha$ -1	2.540	2.70	7.18	22.381	0.957	6.76	14.11		8948.8

<sup>a</sup> Energy of the inflection point in the first differential XANES.

**Table S10.** Ln-O<sub>H<sub>2</sub>O</sub> distances for the K<sup>+</sup>-Ln- $\alpha$ -1 series of solid salts and aqueous solutions as well as the corresponding average Ln-O<sub>H<sub>2</sub>O</sub> distances for the TBA<sup>+</sup>-Ln- $\alpha$ -1 series of solid salts and acetonitrile solutions as obtained from the two-shell EXAFS analyses. The intrasystem distance differences ( $\delta = 0.00\text{--}+0.06 \text{ \AA}$ ) between the MeCN solutions and the parent TBA<sup>+</sup> salts as well as the average intersystem differences ( $\Delta = +0.01\text{--}+0.05 \text{ \AA}$ ) between the MeCN solutions of TBA<sup>+</sup>-Ln- $\alpha$ -1 and the corresponding aqueous solutions of K<sup>+</sup>-Ln- $\alpha$ -1 support a fractional exchange of H<sub>2</sub>O with MeCN pursuant to Eq. (1) in the article.

Ln- $\alpha$ -1 (Z)	Ln-O <sub>H<sub>2</sub>O</sub> Distances and Distance Differences						Intersystem Differences <sup>b</sup>	
	K <sup>+</sup> systems			TBA <sup>+</sup> systems			Salts	Solns
	K <sup>+</sup> Salts	H <sub>2</sub> O Solns	$\delta, \text{\AA}^a$	TBA <sup>+</sup> Salts	MeCN Solns	$\delta, \text{\AA}^a$	$\Delta, \text{\AA}^b$	$\Delta, \text{\AA}^b$
Nd (60)	2.55(2)	2.56(3)	+0.01	2.58(2)	2.60(2)	+0.02	+0.03	+0.04
Sm (62)	2.48(4)	2.48(3)	0.00	2.45(2)	2.51(3)	+0.06	-0.03	+0.03
Eu (63)	2.50(5)	2.48(5)	-0.02	2.46(1)	2.49(3)	+0.03	-0.04	+0.01
Tb (65)	2.37(2)	2.39(4)	+0.02	2.39(5)	2.42(6)	+0.03	+0.02	+0.03
Dy (66)	2.37(2)	2.35(3)	-0.02	2.37(3)	2.37(8)	0.00	0.00	+0.02
Yb (70)	2.31(2)	2.29(7)	-0.02	2.30(1)	2.34(6)	+0.04	-0.01	+0.05

<sup>a</sup> Distance difference = solution – salt. <sup>b</sup> Distance difference = TBA<sup>+</sup> – K<sup>+</sup>.

## References

- W. R. Heineman and P. T. Kissinger, in *Laboratory Techniques in Electroanalytical Chemistry*, eds. P. T. Kissinger and W. R. Heineman, Marcel Dekker, New York, 1996, pp. 51-125.
- P. Mialane, L. Lisnard, A. Mallard, J. Marrot, E. Antic-Fidancev, P. Aschelhoug, D. Vivien and F. Secheresse, *Inorg. Chem.*, 2003, 42, 2102-2108.
- M. R. Antonio, B. K. Teo and B. A. Averill, *J. Am. Chem. Soc.*, 1985, 107, 3583-3590.
- B. K. Teo, M. R. Antonio and B. A. Averill, *J. Am. Chem. Soc.*, 1983, 105, 3751-3762.
- C. Boglio, G. Lenoble, C. Duhayon, B. Hasenknopf, R. Thouvenot, C. Zhang, C. Howell R., P. Burton-Pye B., C. Francesconi L., E. Lacote, S. Thorimbert, M. Malacria, C. Afonso and J.-C. Tabet, *Inorg. Chem.*, 2006, 45, 1389-1398.

6. Q. H. Luo, R. C. Howell, M. Dankova, J. Bartis, C. W. Williams, W. D. Horrocks, V. G. Young, A. L. Rheingold, L. C. Francesconi and M. R. Antonio, *Inorg. Chem.*, 2001, 40, 1894-1901.
7. M. Sadakane, M. H. Dickman and M. T. Pope, *Inorg. Chem.*, 2001, 40, 2715-2719.
8. J. Mink, M. Y. Skripkin, L. Hajba, C. Nemeth, A. Abbasi and M. Sandstrom, *Spectroc. Acta Pt. A-Molec. Biomolec. Spectr.*, 2005, 61, 1639-1645.
9. W. W. Lukens, J. J. Bucher, D. K. Shuh and N. M. Edelstein, *Environ. Sci. Technol.*, 2005, 39, 8064-8070.